Novel Growing Robot With Inflatable Structure and Heat-Welding Rotation Mechanism

Yuki Satake, Atsuo Takanishi, *Fellow, IEEE*, and Hiroyuki Ishii, *Member, IEEE*

***Abstract*—Soft robotics has recently become a popular topic owing to its advantages over conventional rigid robotics. In this article, we introduce a soft robot that can grow with its own structure; its main components include an inflatable tube for its body and a tip with an expansion mechanism. The tube is made of conventional laminated film. It leads the robot to improved applicability. The robot can grow along the horizontal and vertical directions, and it can bend around yaw and pitch axis. To achieve this, a mechanism feeds air into the inflatable tube for growing the structure, and another heat welding mechanism allows producing bending points where necessary. The experimental results confirm that the proposed robot can grow in mid-air and bend around the yaw axis with varying bending radii. Further, the robot can climb a wall and displace an upper surface by pitch-axis bending. The designed bending structures are very stable because of heat welding; the growing and climbing capabilities depend on the inner pressure of the tube, and these capabilities allow the robot to select various shapes and move seamlessly in various environments.**

***Index Terms*—Growing robots, mechatronics, mobile robots, pneumatic systems, soft robotics.**

Manuscript received January 7, 2020; revised March 26, 2020; accepted April 29, 2020. Date of publication June 2, 2020; date of current version August 13, 2020. This work was supported by Fluid Power Technology Promotion Foundation, JST, and JSPS KAKENHI under Grant 15K00366, Grant 17H00767, Grant 19H01130, and Grant 25220005. Recommended by Technical Editor J. Kober and Senior Editor X. Chen. *(Corresponding author: Hiroyuki Ishii.)*

Yuki Satake is with the Department of Modern Mechanical Engineering, Waseda University, Tokyo 169-8050, Japan (e-mail: yuki.sa417@toki.waseda.jp).

Atsuo Takanishi and Hiroyuki Ishii are with the Human Robotics Institute (HRI), Waseda University, Tokyo 169-8050, Japan (e-mail: takanisi@waseda.jp; hiro.ishii@waseda.jp).

This paper has supplementary downloadable material available at http://ieeexplore.ieee.org, provided by the author. There are two videos. The first video, titled YawBending.mp4, shows the yaw-axis bending experiment. The robot grew in length and stopped growing to weld the tube for rightward bending. The robot then grew for 8 seconds (tg=8). After that, the tube was welded for rightward bending again. Overall, we set four bending points and the bending radius became 200 mm. The second video, titled PitchBending.mp4, shows the demonstration that the robot passed over a box using two pitch rotations. The robot grew towards the box. It stopped growing when the tip machine touched the box, and welding started for pitch-axis bending. After welding, the robot grew again. The robot welded the tube for pitch-axis bending, again, when it reached the top of the box. The robot moved on the surface of the box after the second bending to continue its motion over the obstacle.

Color versions of one or more of the figures in this article are available online at https://ieeexplore.ieee.org.

Digital Object Identifier 10.1109/TMECH.2020.2999467

I. Introduction

SOFT robotics has recently become one of the most active research fields in robotics given its potential to allow safe contact with humans and the environment. Several studies have focused on soft robotic manipulators with multiple degrees of freedom. Tendon-driven [1]–[6] and pneumatic [7]–[13] mechanisms enable soft manipulators to ensure safe interactions with humans and the environment. Besides softness, these manipulators provide several advantages over their conventional rigid counterparts, including being lightweight and environmentally adaptable. Most soft manipulators have either multiple degrees of freedom or a continuum body, and thus, they can adapt their shapes and postures to their surroundings such as ground surfaces, walls, and objects, using corresponding physical interactions. Simulations of soft manipulators are usually conducted to understand adaptation mechanisms because this process is difficult to understand only using conventional mechanics models. Furthermore, simulation studies contribute to precise control [1], [2].

Soft robotic mechanisms that allow growth have been devised in recent years. For example, Dehghani *et al*. [14] developed an eversion robot for application in colonoscopy, whereas Saxena *et al*. [15] developed an eversion robot for endoscopy. Luong *et al*. [16] developed an eversion robot for underwater operation; the robot was designed by allowing contact between the robot body and the environment. Blumenschein *et al*. [17]–[19] developed a robot that extends from its tip. Some of these robots have three series pneumatic artificial muscles (PAMs) or three series of pouch motors attached to its body, which enable the robot to steer reversibly. Furthermore, certain soft robots have mechanisms that can form the structure by employing a growing mechanism. The robot developed by Hawkes *et al*. [20] grows and bends by inflating a tube consisting of two-layer films. In their research, they used latches to hold the outer layer in a shortened configuration until the latch was popped open by the inflation of the chamber between the inner and outer layers, which allowed the outer layer to increase in size. The robot developed by Sadeghi *et al*. [21], [22] grows and bends by melting a thermoplastic filament and solidifying it back to form the required shape, thereby resembling a three-dimensional (3D) printer; this robot is powerful enough to displace itself through the soil. Such robots can change the direction of the tip growth in real time as they can take arbitrary shapes. Therefore, they are expected to enable the development of novel approaches for construction that allow safe contact with the environment,

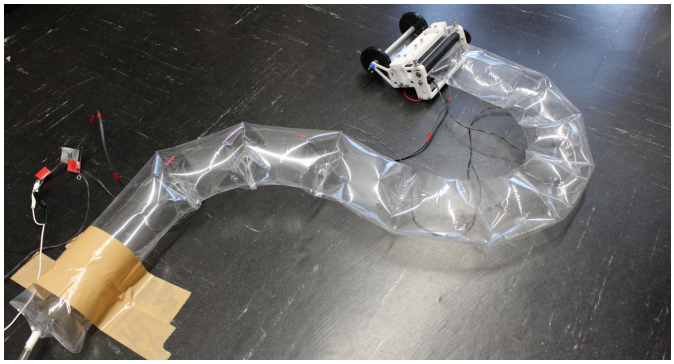

Fig. 1. Proposed soft robot in this article.

and they can be applied to design a variety of solutions including flexible antennas, manipulators, and mobile robots for inspecting narrow spaces such as caves. Therefore, we believe that further research should be conducted on growing robots with changing and adaptable shapes.

Inflatable structures are popular among soft manipulators and may be promising for growing robots that increase their volume. Such structures consist of soft tubes or chambers that can be inflated with air or other gasses, and their major advantages include adaptability and light weight. Thus, inflatable structures are used in construction and civil engineering fields. For example, inflatable rubber dams and silt fences are often used for water control [23], [24]. Inflatable structures can be used for temporary constructions such as tents and antennas [25], [26]; furthermore, they can be used to construct large structures given their light weight [27]. Large-scale robots have been constructed using inflatable structures [28], [29]. Overall, inflatable structures are adaptable, portable, and safe; therefore, they are suitable to design appropriate solutions for humans and the environment.

The adoption of inflatable structures for mechatronics may be a suitable approach to construct growing robots; thus, in this article, we develop a robot with a growing structure (see Fig. 1). Furthermore, we propose a method for soft inflatable growing robots and report the fabrication of a prototype using this method. The resulting robot can grow horizontally and establish bending points; furthermore, it can grow vertically and bend around the yaw and pitch axes to interact with walls or objects. The developed robot consists of a long inflatable tube made of an elastomer, tube feeding mechanism, heat welding mechanism to establish bending points, and compressor for inflating. The tube is made of conventional film, which helps minimize cost and improve applicability. The robot stores a tube at the tip, and it enables the robot to grow from its tip and move with a small amount of friction between its body and the environment. Real-time heat welding for bending is an especially novel mechanism, and it helps create very stable structures. It enables the robot to turn discretely at any point along the robot and form a wider variety of shapes. In addition, it is safe to use in terms of the environment because the proposed robot can maintain its bending shape without contacting the object. We confirmed that the proposed robot can grow in mid-air as per the inflatable cantilever beam model, and the bending radius can be controlled as per the yaw-axis bending model. The proposed robot can climb a wall by bending around the pitch axis. We developed a model that represents the growing length after pitch-axis bending.

TABLE I
PROPERTIES OF TUBE MATERIALS

Property	Polyethylene	Nylon
Melting point (°C)	110	265
Density (g/cm^3)	0.9	1
Tensile strength (kgf/mm^3)	0.42–1.61	7.7–8.4

The remainder of this article is organized as follows. Section II describes the methods for each robot mechanism and details the model and the fabricated robot prototype. In Section III, we report experimental results to verify the robot performance and discuss them in Section IV. Finally, Section V concludes this article.

II. Design and Fabrication of Soft Robot Mechanisms

In this section, we explain the mechanisms of the proposed soft inflatable robot that comprises three parts: 1) inflatable tube, 2) feeding mechanism, and 3) heat welding mechanism. We then detail the modeling of each mechanism and the fabrication of the soft robot prototype. The prototype robot comprises a tip machine with feeding mechanisms, a structure mechanism with heat welding and a container for the nongrowing tube, the body tube, a pneumatic circuit connected to the tube, an air compressor, a circuit for welding, and the power source systems.

A. Inflatable Tube

The inflatable tube is a columnar long tube made of thin elastomer film. As the tube is inflated with air to alter its structure, it must be sufficiently strong to withstand the inner pressure. As bending points are produced by heat welding, the tube needs to be made of thermoplastic films that have low melting points. However, such thermoplastic films are usually weak and cannot be used for stretching. Thus, we use a double-layer film (laminated film) that consists of two different film materials for the columnar long tube. The inner-layer film has a low melting point, whereas the outer-layer film has a high heat resistance and strength to stretching forces, which provides the structure with the required low melting point and strength. In particular, we use an NY#15/DL/LL#40 polyethylene film that has a low melting point and a stronger nylon film. The 40-μm-thick polyethylene film is placed at the inner side, and the 15-μm-thick nylon film is placed at the outer side; these films are bonded together using an adhesive. The diameter of the tube (Mitsuwa Ltd.) is 76 mm. Table I lists the properties of the employed tube materials.

B. Growing and Feeding Mechanism

When a robot grows with its own structure, the procedure should ideally start from its tip. Irreversible steering caused by using bend points is more logical when a robot grows from the tip rather than from the base because it enables directing the front

of the robot as it moves forward. Furthermore, tip growth allows extension of the robot without relative movement between its body and the environment, which allows navigation through cluttered environments and tortuous paths with relative ease compared to continuum robots that move by sliding their entire body along the environment; therefore, it decreases friction when the robot moves. Growing from the tip can be achieved by either supplying material from the base to the tip [15]–[22] or by storing the material at the tip before use [14], [30]. The former method requires a mechanism to supply the material to the tip, and the latter method requires compactly storing the material to prevent interference with robot operation. As mentioned in Section I, the proposed soft robot has an inflatable structure, which has the advantage of compactness. When a tube is inflated with air, it forms a 3D shape, and the tube can be contained as a film before use. Therefore, we adopted growing by storing the material at the tip and feeding it stepwise while inflating the tube with air for growing.

According to Comer and Levy [31], the transverse buckling load of inflatable tubes depends on their diameter, inner pressure, and length. The maximum transverse buckling load $F_{\mathrm{t\_buckling}}$ is given by

$$F_{\mathrm{t\_buckling}} = \pi p r^3 / L \tag{1}$$

where p is the inner pressure, r is the radius of the tube, and L is the length of the tube. In addition, they found that the minimum moment $M_{\mathrm{t\_slack}}$ that causes the slack region on the tube is given by

$$M_{\mathrm{t\_slack}} = \pi p r^3 / 2. \tag{2}$$

When the slack region occurs, the tube largely loses its stiffness. A tube with no slack region is regarded as a cantilever beam, and the transverse displacement y is described by

$$\frac{d^2 y}{dx^2} = \frac{M}{EI} \tag{3}$$

where E is Young's modulus, I is the second moment of area, and M is the bending moment. Fichter [32] and Le Van and Wielgosz [33] investigated the axial buckling of inflatable tubes. According to Fichter, the axial buckling load of inflatable tubes $F_{\mathrm{a\_buckling}}$ is described by

$$F_{\mathrm{a\_buckling}} = \frac{EI\frac{\pi^2}{L^2}\left(p\pi r^2 + G\pi r t\right)}{EI\frac{\pi^2}{L^2} + p\pi r^2 + G\pi r t} \tag{4}$$

where G is the shear modulus and t is the wall thickness of the tube. These equations show that high inner pressure increases $M_{\mathrm{t\_slack}}$ and $F_{\mathrm{a\_buckling}}$. The proposed robot requires high pressure in the growing tube, whereas the nongrowing tube should not receive air inflow to keep it compact. Therefore, air must be completely cut-off at the boundary between the growing and nongrowing sections. To this end, we used two rollers to establish a nip mechanism. The rollers apply force to cut-off the air in the nongrowing section and feed material by rotating in the growing section, as illustrated in Fig. 2.

Some forces applied to the growing and feeding mechanisms are shown in Fig. 2. When the tube is inflated with air, the roller surfaces in contact with the tube experience force F_{air}, which is

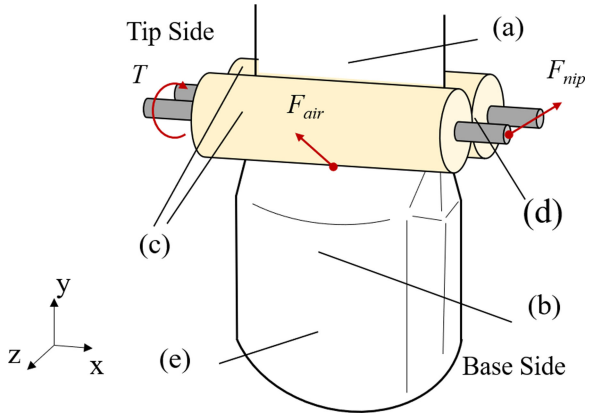

Fig. 2. Overview of the growing and feeding mechanism. (a) Nongrowing section tube with low stiffness. (b) Growing section tube with high stiffness. (c) Rollers for nipping and feeding. (d) Nip part that cuts off air. (e) Tube.

divided into force $F_{\mathrm{air\_y}}$ along the longitudinal direction of the tube (positive y-axis) and force $F_{\mathrm{air\_z}}$ along the perpendicular direction of the tube (positive z-axis). The forces push the rollers in the direction of the growth and widen the distance between rollers. Although the rollers promote motion along the positive y-axis, the sliding friction f between rollers and the tube resists motion. Along the z-axis, the force F_{nip} that the rollers apply should be larger than force $F_{\mathrm{air\_z}}$ ($F_{\mathrm{nip}} > F_{\mathrm{air\_z}}$) for nipping the tube and preventing air inflow into the nongrowing tube section. Yet, a large F_{nip} results in high rolling resistance, and hence, we use a motor to supply torque T for assisting rolling.

C. Bending Mechanism

As mentioned in Section I, the direction of the tip growth can be changed in real time and various shapes can be freely established along with growing. For bending the structure, we adopt heat welding for thermoplastic films. Heat welding has been used for thermoplastic films to create pouch motors [19], [34]; in addition, it is used before the robots are used. The proposed robot uses heat welding while the robot is being used in real time. In addition, pouch motors are used as actuators for contraction or rotation, while the proposed robot uses heat welding to create the bending structure of the body. Yaw axis bending and pitch axis bending can be achieved by using different heat welding procedures, which are described below.

1) Yaw Axis: The tube that constitutes the body can be welded at a point either on the left or right side of the structure before inflating (left graph in Fig. 3). After the tube is fed and it passes through the nip, the tube attempts to form a columnar shape using the inner pressure, and inflation is impeded at the welded part. Therefore, a difference in length along the growing direction between the welded and nonwelded sides appears, and the tube is bent toward the welded side (right graph in Fig. 3). Although the bending angle per welding is not large, it can be increased by repeated welding at different points. When growing and welding are repeated alternately, the body shape forms the sides of a polygon, and the bending radius of the body is approximately represented as the radius of the inscribed circle

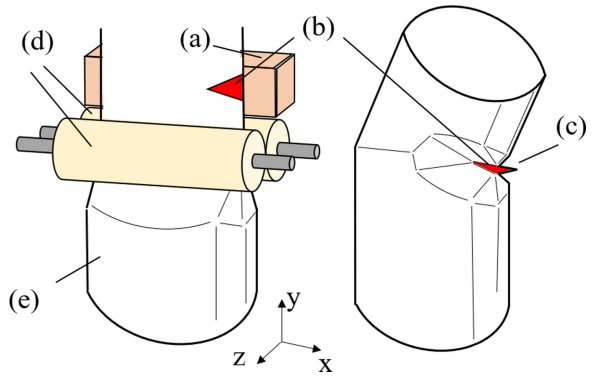

Fig. 3. Overview of yaw-axis bending. The tube is welded before being inflated (left graph). Yaw-axis bending occurs at the welded point after inflation (right graph). (a) Part to modify the structure. (b) Welding point. (c) Bending point. (d) Rollers. (e) Tube.

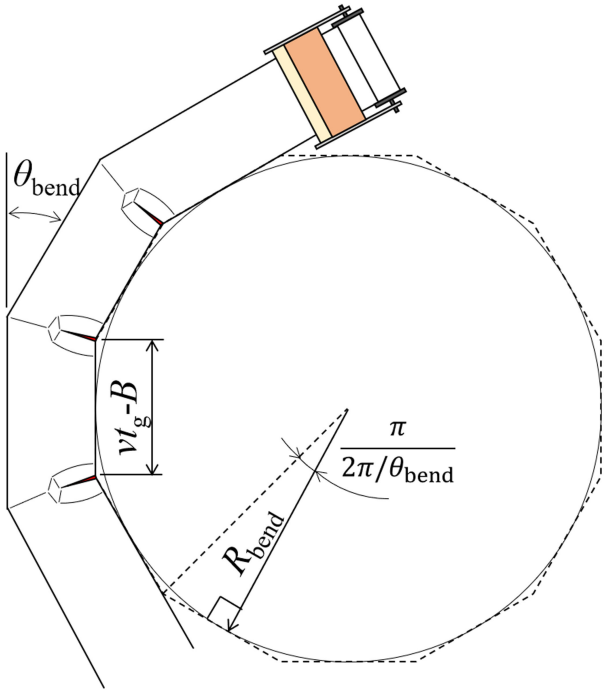

Fig. 4. Bending radius R_{bend} when the polygon is a regular polygon (when the growing times between the heat welding are the same).

of the polygon. As shown in Fig. 4, when the polygon is a regular polygon, the bending radius R_{bend} is given by

$$R_{\text{bend}} = \frac{vt_{\text{g}} - B}{2\tan\left(\frac{\pi}{2\pi/\theta_{\text{bend}}}\right)} \tag{5}$$

where v is the growing speed (feeding speed) of the robot, t_g is the growing time between the heat welding, B is the width of the welding (the base of the welding triangle in Fig. 3), and θ_{bend} is the bending angle per welding.

2) Pitch Axis: Pitch-axis bending cannot be welded like yaw-axis bending because the tube is stored in a flat state. A line is welded in the tube along the direction perpendicular to the tube longitudinal direction around the central axis (left graph in Fig. 5). Thus, part of the tube around the central axis is prevented from inflating, with the left and right sides being

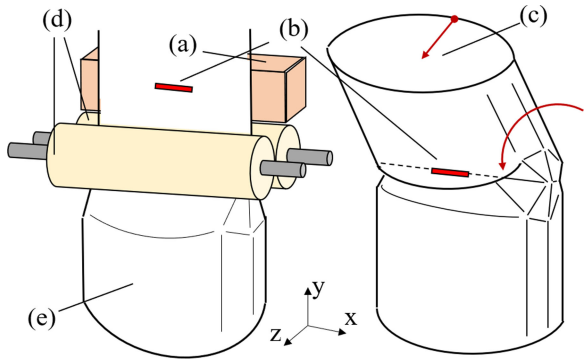

Fig. 5. Overview of pitch-axis bending. The tube is welded before being inflated (left graph). Pitch-axis bending occurs at the welded point after inflation and when the tube has a force applied along the z-axis (right graph). (a) Part to modify the structure. (b) Welding point. (c) External force along z-axis. (d) Rollers. (e) Tube.

inflated; consequently, the tube has stiffness around the yaw axis (although smaller than the original stiffness). However, the total cross-sectional area becomes smaller, and the tube loses stiffness around the pitch axis. When applying force along the z-axis to the tube after the welding, it produces the desired bending.

When the robot is growing, the first part that touches an obstacle is the one that contains the nongrowing tube. Then, rotation by feeding the rolled tube enables pitch-axis bending. Side plates in the regions containing the rolled tube are used as wheels, exerting friction F_{t_z} along the positive z-axis by torque T_t obtained from the rotation with the tube feeding at contact points with the obstacle. Therefore, a pitch rotation occurs at the welded point, and the growing direction changes. The resultant force from F_{t_z} and the driving force F_{air} generated by air pressure and roller rotation at the nip part of the growing and feeding mechanism are larger than the friction between other parts of the robot and wall, as well as the gravity acting on the tip machine, producing growth along the z-axis. As growing progresses, the angle between the ground and the tube after bending increases, and hence, F_{air} provides growing without the contact force F_{t_z} between the part containing the nongrowing tube and the obstacle.

D. Prototype of Tip Machine

We integrated all robot components to fabricate a prototype, whose tip is shown in Fig. 6. In the growing and feeding mechanism, polyurethane rollers with a shore A hardness of 50 and diameter of 15 mm were used to establish the nip part. Bolts apply force F_{nip} to the upper roller at both ends of the shaft, which makes the rollers nip the tube and cut-off airflow. A motor (Maxon motor, RE16 and GP16C gear head) of 4.5 W driven by 7.5 V was used to assist the lower roller rotation. Two gears fixed on the motor shaft and the bottom roller shaft, respectively, were used to transmit the torque and total reduction ratio that includes the motor gear head was 471:1. The tube feeding speed v of the fabricated mechanism was 18 mm/s when the inner pressure is 10 kPa.

To create the structure mechanism, nichrome wires 0.2 mm in diameter were used for heat welding by arranging them as

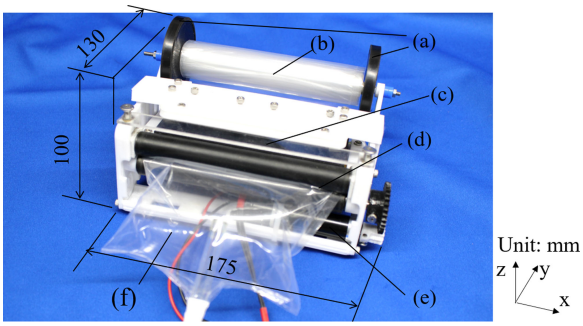

Fig. 6. Fabricated tip machine. (a) Rubber sheet attaching side plates. (b) Tube container. (c) Part for making structure by heat welding. (d) Nip part composed of two rollers for cutting-off airflow and feeding the tube. (e) Motor for assisting roller rotation. (f) Tube constituting the robot body.

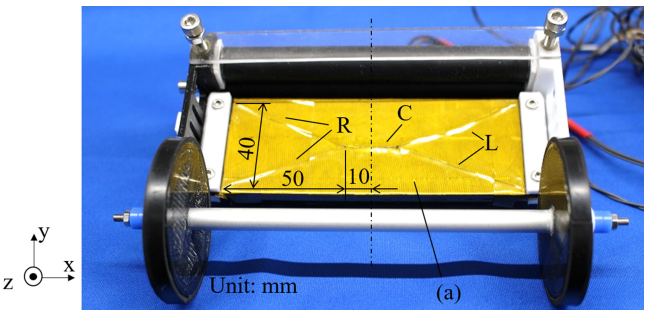

Fig. 7. Arrangement of nichrome wires. (a) Yellow polyimide tape that wraps the plate. Nichrome wires labeled with R, L, and C correspond to the respective heating wires in the circuit of Fig. 8.

hypotenuses of the isosceles triangle whose base is 40 mm and height is 50 mm for yaw-axis bending, and a 20 mm line is used for pitch-axis bending (see Fig. 7). Heat welding by this arrangement creates a 30° bending angle for yaw-axis bending. The bending angle depends on the arrangements of nichrome wires, and we chose this arrangement from many trial results. The left and right wires for yaw-axis bending were activated using 3.2 V and 1.9 A for 6 min, respectively; the wire temperature increased to 145 °C. They make two welded lines that meet each other at an angle. The center wire for pitch-axis bending was activated using 1.75 V and 1 A for 6 min, reaching a temperature of 135 °C; this creates one welded line. The nichrome wires were placed on a polycarbonate plate that wrapped a heat-resistant glass cloth tape, and a polyimide tape was wrapped on them. The tape prevents the nichrome wires from changing their shape and reduces friction in the tube to promote sliding. Pressure was provided above the heat welding part; a compressive force was applied to the tube, where the force is provided by bolts.

Rubber sheets were attached to the side plates of the tube container, and they increased friction between the containers and the obstacles for pitch-axis bending. Other parts—gears and side plates—were 3D-printed in polycarbonate. The weight of the fabricated tip machine was 491 g.

E. Additional Components

Fig. 8 shows the circuit including the nichrome wires for heat welding, which is achieved by combining four switches

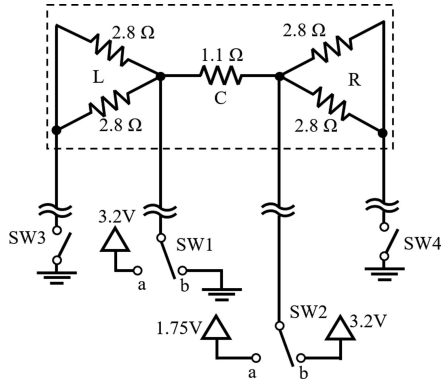

Fig. 8. Circuit for heat welding. Heating wires labeled with R, L, and C correspond to the respective nichrome wires indicated in Fig. 7. The circuit part surrounded by the dashed rectangle is mounted on the tip machine and connected to the power sources and ground with four long lead wires.

TABLE II
SWITCH COMBINATIONS FOR HEAT WELDING

Direction	SW1	SW2	SW3	SW4
Left	a	Off	On	Off
Right	Off	b	Off	On
Pitch	b	a	Off	Off

per bending by using the combinations listed in Table II. In addition, the pneumatic circuit is composed of a regulator, pressure gauges, three ball valves, an air compressor (EARTH MAN, EM oil-less air compressor, max flow rate of 15 L/min), and a tank. Air is discharged when the robot is not growing and pressure is not required (e.g., when the robot is heat welding). A urethane tube is used as a pipeline.

III. Experiments and Results

A. Transverse Buckling and Growing

We first conducted an experiment to evaluate the transverse buckling load and horizontal growth of the robot. The base of the robot was fixed to a stand, and the robot grew outwards from the stand. We measured the vertical displacement of the tip machine by gravity every 50 mm of growth. The growing length was defined as the distance between the edge of the stand and the nip part. The robot stopped growing when large wrinkles appeared in the tube and the robot could not grow horizontally. The inner pressure in the tube was varied from 8 to 20 kPa in increments of 4 kPa. The experiments were repeated six times for each inner pressure. Fig. 9 shows the results of this experiment, where the growing length increases at higher inner pressure. The dotted line in Fig. 9 represents the model of (3) and the x-marks show lengths at which the slack region appears in the model (2). The error bars in Fig. 9 represent standard deviations.

B. Yaw-Axis Bending

We conducted another experiment to evaluate the different shapes that can be achieved by yaw-axis bending. In this experiment, the base of the robot was fixed to the floor, and the

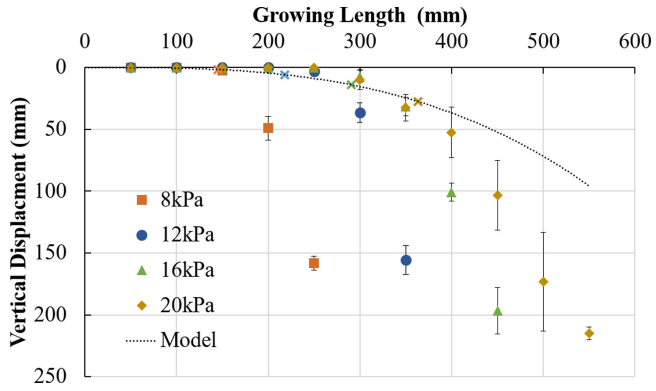

Fig. 9. Transverse buckling and horizontal growing experiment results, where length increases at higher inner pressure. The dotted line represents the beam model (3) and x-marks show lengths that slack region appears (2). The error bars represent standard deviations.

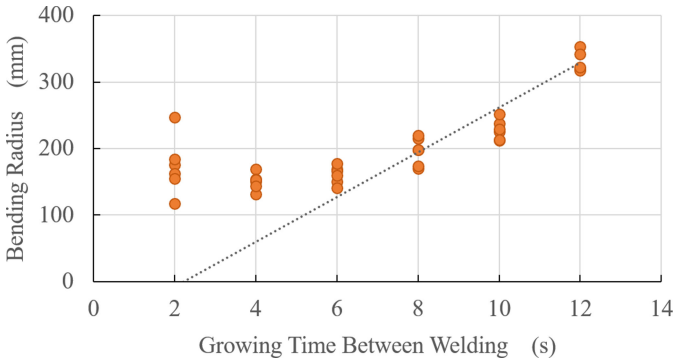

Fig. 10. Yaw-axis bending experiment results. The bending radius increases at a long growing time in 6-12 s. The dotted line represents the bending radius model. The growing time corresponds with the distance between welds.

robot grew in length. It stopped growing to weld the tube for rightward bending, and then, the robot grew for t_g s. After t_g s, the tube was welded for rightward bending. Overall, we set four bending points and measured the bending radius formed by the robot. We repeated the experiment while changing t_g from 2 to 10 s at increments of 2 s; the inner pressure is 10 kPa in all t_g experiments. Figs. 10 and 11 show the result of this experiment; the dotted line in Fig. 10 represents the bending radius model (5).

C. Pitch-Axis Bending

We finally conducted an experiment to evaluate the robot ability to climb a wall by pitch-axis bending. The base of the robot was again fixed to the floor, and the robot grew toward a wall. It stopped growing when the tip machine touched the wall, and welding started for pitch-axis bending. After welding, the robot grew again. We investigated whether the robot was able to climb the wall and measured the growing length along the vertical direction. When the robot fell, the experiment was concluded. We conducted the experiment while changing the inner pressure of the tube from 8 to 14 kPa in increments of 2 kPa. Figs. 12 and 13(a) show the result of this experiment,

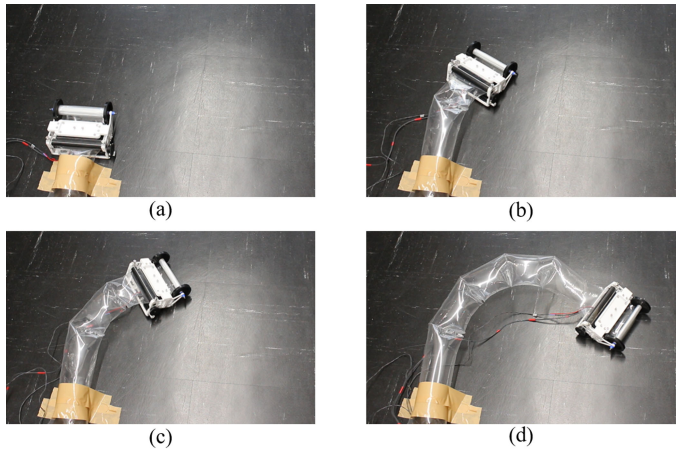

Fig. 11. Yaw-axis bending experiment sequence ($t_g = 8$ s): (a) before growing and after (b) first, (c) second, and (d) fourth bending.

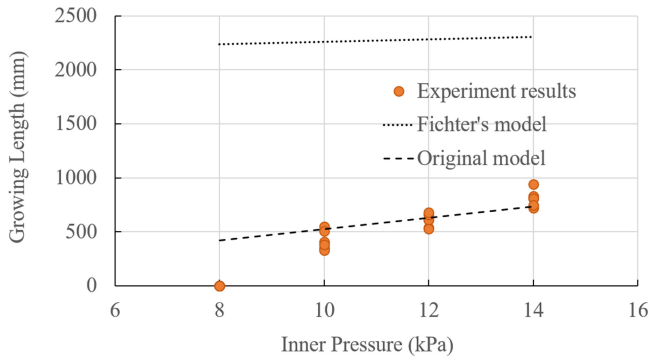

Fig. 12. Pitch-axis bending experiment results. When the inner pressure is 8 kPa, the robot cannot climb the wall. When the inner pressure is above 10 kPa, the growing length increases at higher inner pressure. However, results fall far short of the length of Fichter's model (4) (dotted line). The broken line represents the original model (9).

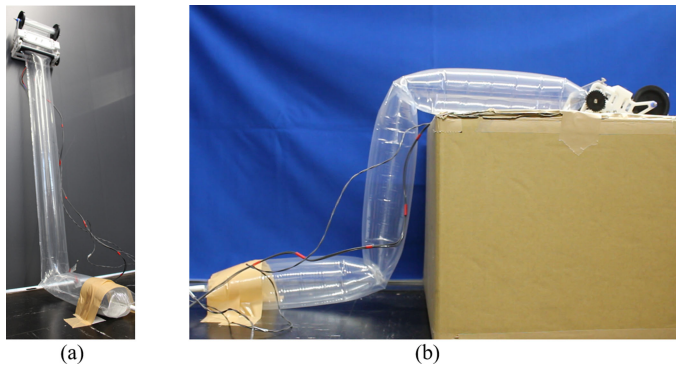

Fig. 13. (a) Pitch-axis bending experiment when the robot grows to 700 mm at inner pressure of 14 kPa. (b) Passing over a box using two pitch rotations. The robot moves on the surface of the box after the second bending to continue its motion over the obstacle.

where the robot cannot bend, grow, and climb the wall at an inner pressure of 8 kPa. For an inner pressure of 10 kPa or above, it can bend around the pitch axis and grow to climb the wall as the inner pressure increases. However, the results fall far short of

the length of Fichter's model (4) represented by the dotted line in Fig. 12.

IV. Discussion

In the horizontal growing experiment, we confirmed that high inner pressure increases the transverse buckling load of the tube, which enables the robot to grow longer. Hence, the transverse buckling load can be controlled by inner air pressure. In addition, the tube deformation corresponds with the model of the cantilever beam (3) before the slack region appears. These results agree with Comer and Levy's findings [31]. Therefore, the proposed robot can grow stably with a small vertical displacement, which is estimated using (3), before the slack region appears. We confirmed this fact and that the model must be used to select a pass with gaps in the rough ground because they help us decide whether the robot can step over gaps or not.

The horizontal growing length in mid-air of the proposed robot can be estimated from the diameter of the tube and its inner pressure, and it can be further increased using inner pressures above 16 kPa; however, we did not apply such high pressures in the prototype to prevent air leaks at the roller and bursts of welding points. Thus, we set the maximum applicable pressure for our robot to 16 kPa, which is similar to the pressure in the inflatable growing structure developed by Coad *et al.* [19] (i.e., 14–21 kPa). Note that burst pressure depends on the tube material, and stronger tubes with enough softness would allow the application of higher pressure, which would increase the growing speed and length. Moreover, when some support exists, the robot can grow much longer.

The growing speed of the proposed robot is 18 mm/s under 10 kPa (when adding the time required to wait for the sealing to occur, the average growth speed is much slower), whereas that of the robot developed by Sadeghi *et al.* [22] is 3–4 mm/s; by Coad *et al.* [19] is 100 mm/s. Furthermore, the max speed over short distances for the robot developed by Hawkes *et al.* [20] is 10 m/s. Thus, the growing speeds of robots with inflatable structures are higher than that of robots with additive manufacturing technologies. The experiment results suggest that the proposed inflatable growing robot can step over gaps on the ground, which are mostly impossible to handle for wheeled robots, whose size is comparable to that of the tip module.

The results for t_g in 6–12 s from the yaw-axis bending experiment suggest that the bending radius changes as per model (5). However, results for t_g in 2–4 s are larger than the model because the distance between welding points, which is very short, impedes air filling and proper bending. Thus, the bending angle θ_{bend} becomes smaller, and the bending radius becomes larger. Hence, the bending radius can be changed by adjusting the growing time for t_g after 6 s. When the inner pressure is not 10 kPa, the growing speed v changes from 18 mm/s. Therefore, the bending radius becomes different from these results for the same t_g. Thus, the bending radius can be estimated by model (5) if the growing speed v is measured at the other inner pressure. Hence, the minimum bending radius of the fabricated prototype that can be achieved in a stable manner is 161 mm for $t_g = 6$ s under 10 kPa.

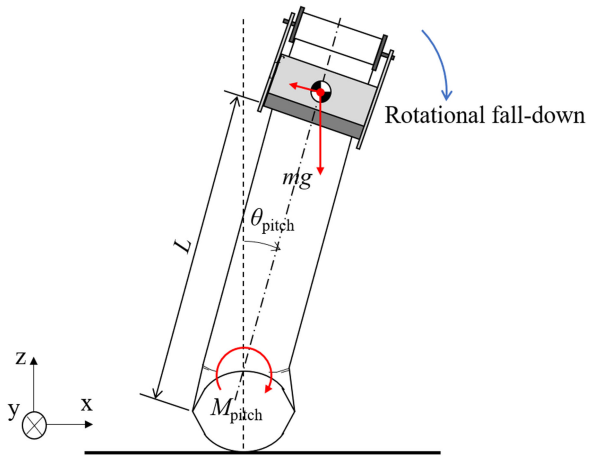

Fig. 14. Model for pitch-axis bending. Rotational fall-down occurs.

The proposed robot resembles a continuum structure given its variable bending radius. Moreover, our robot can control the radius during growing by repeatedly bending. Furthermore, as our robot can grow, which is not possible in conventional continuum robots, it can form a wider variety of shapes. Yet, the minimum bending radius with a shorter t_g is limited by the distance between the welding points. Hence, the minimum bending radius of the proposed robot is larger than that in other studies, about 100 mm in [21] and 90 mm in [20] (this value is estimated by the figures provided in these papers). The minimum bending radius of the proposed robot is smaller than the robot developed by Greer *et al.* [18] (300 mm). In addition, the proposed bending mechanism can be modified to further reduce the bending radius by using tubes with a smaller diameter.

The results from the pitch-axis bending experiment confirm that the growing length increases with inner pressure. However, the tube fell down before reaching the buckling lengths; hence, the results do not agree with Fichter's model (4). The difference between the experimental results and the model is caused because of the rotational fall-down of the tube around the bending point, as shown in Fig. 14, which occurred before buckling. This rotational fall-down seems to occur because the bending point is not fixed and the robot does not climb a wall along the precisely vertical direction. As shown in Fig. 12, the varieties in the maximum reaching heights after pitch-axis bending between trials under the same conditions are small, and we consider that rotational fall-down occurs with high reproducibility. We then developed a model for rotational fall-down. Geometric modeling around the welding point was considered at first. However, such modeling is very complex and difficult because of the complex interactions of design parameters such as the tube material and welding shape. We then employed another approach to model the rotational fall-down as described below. Rotational fall-down of the tube always occurs near the welding point on the tube because the cross-sectional shape changes. Therefore, a model was developed by referring to Comer and Levy's model (1) and (2). Although the robot should ideally grow along the precisely vertical direction, the robot does not do that in reality and is slightly inclined, as shown in Fig. 14. Hence, the tube starts

rotating around the bending point. In the case of transverse buckling, the maximum moment M_{stand} that does not cause buckling on the tube is given by (6) derived from (1)

$$M_{\mathrm{stand}} = \pi p r^3 . \tag{6}$$

Considering that the rotational fall-down develops on the tube around pitch-axis bending, which can be considered as two closed tubes connected by a line, the maximum moment M_{pitch} that does not cause rotational fall-down on the tube must be smaller than M_{stand}. Therefore, M_{pitch} can be modeled as shown in (7) using k, which is an allowable moment decline coefficient. This coefficient seems to depend on materials of the tube and the shape of the welding point, while developing a prediction model of the coefficient from the design parameters is difficult because of the complexities of interactions of these parameters. Therefore, this coefficient should be obtained from the experiments such as friction coefficient or air resistance coefficient

$$M_{\mathrm{pitch}} < k M_{\mathrm{stand}} \tag{7}$$

$$M_{\mathrm{pitch}} = mgL \sin\theta_{\mathrm{pitch}} - fL \tag{8}$$

where m is the mass of the tip, g is the acceleration due to gravity, L is the growing length after pitch-axis bending, θ_{pitch} is the inclination of the tube, and f is the friction between the tip and a wall. Equations (7) and (8) give

$$L < k\pi p r^3 \,/\, (mg \sin\theta_{\mathrm{pitch}} - f) . \tag{9}$$

In the experiment described in Section III-C, f is much smaller than $mg\sin\theta_{\mathrm{pitch}}$ because the wall that supports the tube and the mechanism has a smooth surface. θ_{pitch} was 10°; hence, the coefficient k, which is calculated from the experimental result, was 0.243. The broken line in Fig. 12 represents model (9) and agrees with the experimental result. When the friction between the tip and a wall is not small, the friction acts in the direction to prevent falling. Therefore, the actual growing length does not become smaller than L estimated by (9). Thus, predicting the maximum height after pitch-axis bending using this model is helpful when a user navigates the robot in real applications. This model cannot be applied when the inner pressure is less than 8 kPa because the tube cannot be considered as a beam structure.

The robot grew vertically and reached 800 mm in height at 14 kPa. Hence, the proposed inflatable growing robot can climb steps or vertical objects shorter than 800 mm. By making several pitch-axis bending points, the robot can climb over steps as shown in Fig. 13 (b). Therefore, the proposed robot can be used in environments that are difficult to navigate for conventional wheeled robots or soft robotic manipulators.

Besides the abovementioned characteristics, the proposed soft robot uses conventional laminated tubes, while other studies required tubes with special design and fabrication [20]. Therefore, the proposed robot can lead to reduced costs and, thus, improved applicability.

Based on the abovementioned points, the proposed soft robot has the following characteristics. The proposed robot grows from the tip and can move with much less relative movement between its body and the environment than conventional soft robots [1]–[13]. It allows easy navigation through cluttered environments and tortuous paths and growing in very long length. Unlike some growing robots [15]–[22], the proposed robot has no friction of the transporting tube from the base because it stores a new tube at the tip. Therefore, the proposed robot can grow into highly curved shapes with many turns more easily because the pressure required for the growth of some pneumatically growing robots increases with the angle through which they turn [17]. In addition, the proposed robot can store the tube in only the required length, although some robots need longer materials for transport. Furthermore, when a tube that is too long is stored at the tip, it increases the mass at the tip. Thus, the growing speed becomes slower, and the length at which buckling occurs becomes shorter. The proposed robot uses heat welding to create a bent structure in real time. Thus, it is an especially novel point for the proposed robot, and it enables the robot to turn discretely at any point along the robot. Although some reversible steering robots using tendons or PAM [16]–[19] need contact with objects to maintain the bending shape, the proposed robot can maintain the bending shape around the yaw axis without contact with the object; this enables safer use for the environment. The grown body can be used for structures such as fences. Heat welding is a widely used technology in itself, and the bending points made by heat welding are hardly peeled off by external forces. Therefore, it seems more stable and superior to maintain the shape than use latches [20]. However, using the latch mechanism has advantages over the heat welding mechanism; for example, it enables the reuse of a tube with latches, and it does not need something at the robot tip. The growing speed is faster than that of robots such as the 3D printer [21], [22]; thus, the proposed robot can create a structure quickly. However, the proposed robot needs a wall to bend around the pitch axis and grow along the vertical direction. Hence, it is inferior to other steerable robots [17]–[22] in one bending degree of freedom. Moreover, the proposed robot currently has no cameras. Therefore, it does not have navigation capabilities that some robots possess [17]–[20]. The tip machine of the proposed robot has space to mount cameras, and hence, navigation capabilities can be improved. In addition, there is room for improvement of welding shapes because geometric modeling is too complex and difficult around the welding point and cannot be performed currently.

We are working to improve the performance of the proposed robot. For instance, we aim to reduce the weight of the tip machine to grow longer using the same tube and inner pressure used in this article. Moreover, we are developing shape control methods by using computer-aided engineering software.

V. Conclusion

We proposed a method to develop an inflatable growing soft robot and reported the fabrication of a prototype. The proposed robot can grow by feeding a tube and rotate by setting bending points with heat welding, as confirmed experimentally. The mechanism and advantages of the proposed method are discussed, and we demonstrate the capabilities of the proposed method for developing inflatable growing soft robots that may outperform existing structures and approaches.

References

[1] F. Maghooa, A. Stilli, Y. Noh, K. Althoefer, and H. A. Wurdemann, "Tendon and pressure actuation for a bio-inspired manipulator based on an antagonistic principle," in *Proc. Int. Conf. Robot. Automat.*, 2015, pp. 2556–2561.

[2] R. J. Roesthuis and S. Misra, "Steering of multisegment continuum manipulators using rigid-link modeling and FBG-based shape sensing," *IEEE Trans. Robot.*, vol. 32, no. 2, pp. 372–382, Apr. 2016.

[3] L. Zhang, M. Xu, and H. Yang, "Research on soft manipulator actuated by shape memory alloy (SMA) springs," in *Proc. IEEE Int. Conf. Real-time Comput. Robot.*, 2017, pp. 74–78.

[4] Z. Li, L. Wu, H. Ren, and H. Yu, "Kinematic comparison of surgical tendon-driven manipulators and concentric tube manipulators," *Mechanism Mach. Theory*, vol. 107, pp. 148–165, Jan. 2017.

[5] H. Wang, C. Wang, W. Chen, X. Liang, and Y. Liu, "Three-dimensional dynamics for cable-driven soft manipulator," *IEEE/ASME Trans. Mechatronics*, vol. 22, no. 1, pp. 18–28, Feb. 2017.

[6] M. Hwang and D. Kwon, "Strong continuum manipulator for flexible endoscopic surgery," *IEEE/ASME Trans. Mechatronics*, vol. 24, no. 5, pp. 2193–2203, Oct. 2019.

[7] R. Qi, A. Khajepour, W. Melek, T. L. Lam, and Y. Xu, "Design kinematics, and control of a multijoint soft inflatable arm for human-safe interaction," *IEEE Trans. Robot.*, vol. 33, no. 3, pp. 594–609, Jun. 2017.

[8] S. Sanan, M. H. Ornstein, and C. G. Atkeson, "Physical human interaction for an inflatable manipulator," in *Proc. Ann. Int. Conf. IEEE Eng. Med. Biol. Soc.*, 2011, pp. 7401–7404.

[9] X. Peng, N. Zhang, L. Ge, and G. Gu, "Dimension optimization of pneumatically actuated soft continuum manipulators," in *Proc. IEEE Int. Conf. Soft Robot.*, 2019, pp. 13–18.

[10] W. Chen, C. Xiong, C. Liu, P. Li, and Y. Chen, "Fabrication and dynamic modeling of bidirectional bending soft actuator integrated with optical waveguide curvature sensor," *Soft Robot.*, vol. 6, no. 4, pp. 495–506, Mar. 2019.

[11] M. Cianchetti, T. Ranzani, G. Gerboni, I. D. Falco, C. Laschi, and A. Menciassi, "STIFF-FLOP surgical manipulator: Mechanical design and experimental characterization of the single module," in *Proc. IEEE/RSJ Int. Conf. Intell. Robots Syst.*, 2013, pp. 3576–3581.

[12] W. McMahan *et al.*, "Field trials and testing of the OctArm continuum manipulator," in *Proc. IEEE Int Conf. Robot. Automat.*, 2006, pp. 2336–2341.

[13] D. Drotman, M. Ishida, S. Jadhav, and M. T. Tolley, "Application-driven design of soft, 3-D printed, pneumatic actuators with bellows," *IEEE/ASME Trans. Mechatronics*, vol. 24, no. 1, pp. 78–87, Nov. 2018.

[14] H. Dehghani *et al.*, "Design and preliminary of a self-steering, pneumatically driven colonoscopy robot," *J. Med. Eng. Technol.*, vol. 41, no. 3, pp. 223–236.

[15] A. Saxena, E. M. Pauli, R. S. Haluck, B. Fell, and J. Moore, "Tubular locomotion and positioning using tip eversion for endoscopy," *ASME. J. Med. Devices*, vol. 14, 2020, Art. no. 021004.

[16] J. Luong *et al.*, "Eversion and retraction of a soft robot towards the exploration of coral reefs." in *Proc. 2nd IEEE Int. Conf. Soft Robot.*, 2019, pp. 801–807.

[17] L. H. Blumenschein, A. M. Okamura, and E. W. Hawkes. "Modeling of bioinspired apical extension in a soft robot," in *Proc. Conf. Biomimetic Biohybrid Syst.*, 2017, pp. 522–531.

[18] J. D. Greer, T. K. Morimoto, A. M. Okamura, and E. W. Hawkes, "A soft, steerable continuum robot that grows via tip extension," *Soft Robot.*, vol. 6, no. 1, pp. 95–108, 2019.

[19] M. M. Coad *et al.*, "Vine robots: Design, teleoperation, and deployment for navigation and exploration," *IEEE Robot. Automat. Mag.*, early access, Jun. 13, 2019, doi: 10.1109/MRA.2019.2947538.

[20] E. W. Hawkes, L. H. Blumenschein, J. D. Greer, and A. M. Okamura, "A soft robot that navigates its environment through growth," *Sci. Robot.*, vol. 2, no. 8, Jul. 2017, Art. no. eaan3028.

[21] A. Sadeghi, A. Mondini, and B. Mazzolai, "Toward self-growing soft robots inspired by plant roots and based on additive manufacturing technologies," *Soft Robot.*, vol. 4, no. 3, pp. 211–223, Sep. 2017.

[22] A. Sadeghi, E. Del Dottore, A. Mondini, and B. Mazzolai, "Passive morphological adaptation for obstacle avoidance in a self-growing robot produced by additive manufacturing," *Soft Robot.*, vo. 7, pp. 1–10, Oct. 2019, doi: 10.1089/soro.2019.0025.

[23] S. ul Islam and A. Kumar, "Inflatable dams for shp project," *Renewable Sustain. Energy Rev.*, vol. 57, pp. 945–952, May 2016.

[24] P. W. M. Tam, "Use of inflatable dams as agricultural weirs in Hong Kong," *J. Hydraul. Eng.*, vol. 124, no. 12, pp. 1215–1226, Dec. 1998.

[25] O. Girard, F. Brocherie, and G. P. Millet, "On the use of mobile inflatable hypoxic marquees for sport-specific altitude training in team sports," *Brit. J. Sports Medicine*, vol. 47, no. 1, pp. 121–123, Dec. 2013.

[26] L. T. Lowe, P. Gierow, and A. Danis, "Terrestrial based inflatable dish antenna performance characterization," in *Proc. IEEE Antennas Propag. Soc. Int. Symp.*, 2005, pp. 458–461.

[27] C. K. Walker *et al.*, "10 meter sub-orbital large balloon reflector (LBR)," in *Proc. IEEE Aerosp. Conf.*, 2014, pp. 1–7.

[28] M. Takeichi, K. Suzumori, G. Endo, and H. Nabae, "Development of a 20-m-long Giacometti arm with balloon body based on kinematic model with air resistance," in *Proc. IEEE/RSJ Int. Conf. Intell. Robots Syst.*, 2017, pp. 2710–2716.

[29] S. Voisembert, A. Riwan, N. Mechbal, and A. Barraco, "A novel inflatable robot with constant and continuous volume," in *Proc. IEEE Int. Conf. Robot. Automat.*, 2011, pp. 5843–5848.

[30] Z. M. Hammond, N. S. Usevitch, E. W. Hawkes, and S. Follmer, "Pneumatic reel actuator: Design, modeling, and implementation," in *Proc. IEEE Int. Conf. Robot. Autom*, 2017, pp. 626–633.

[31] R. L. Comer and S. Levy, "Deflections of an inflated circular-cylindrical cantilever beam," *AIAA J.*, vol. 1, no. 7, pp. 1652–1655, Jul. 1963.

[32] W. B. Fichter, *A Theory for Inflated Thin-Wall Cylindrical Beams*. Washington, D.C., USA: Nat. Aeronaut. Space Admin., 1966, vol. 3466.

[33] A. Le Van and C. Wielgosz, "Bending and buckling of inflatable beams: Some new theoretical results," *Thin-Walled Struct.*, vol. 43, no. 8, pp. 1166–1187, 2005.

[34] R. Niiyama *et al.*, "Pouch motors: Printable soft actuators integrated with computational design," *Soft Robot.*, vol. 2, no. 2, pp. 59–70, 2015.

Yuki Satake received the B.S. degree in mechanical engineering from the Waseda University, Tokyo, Japan, in 2019, where he is currently working toward the M.S. degree in mechanical engineering.

Atsuo Takanishi (Fellow, IEEE) received the B.S., M.S., and Ph.D. degrees from Waseda University, Tokyo, Japan, in 1980, 1982, and 1988, respectively, all in mechanical engineering.

He is currently a Professor with the Department of Modern Mechanical Engineering, Waseda University.

Dr. Takanishi is a Member and was the President of the Robotics Society of Japan. He is also a Member of the Japanese Society of Biomechanisms, the Japanese Society of Mechanical Engineers, the Japanese Society of Instrument and Control Engineers and the Society of Mastication Systems.

Hiroyuki Ishii (Member, IEEE) received the B.S. and M.S. degree in mechanical engineering and the Ph.D. degree in biomedical engineering from Waseda University Tokyo, Japan, in 2002, 2004, and 2007, respectively.

He is currently an Associate Professor with the Department of Modern Mechanical Engineering, Waseda University. His research interest focuses on interactive robots which induce behavior modifications on humans and animals.

Dr. Ishii was the Recipient of Young Scientists' Prize, The Commendation for Science and Technology by the Minister of Education, Culture, Sports, Science and Technology, Japan, in 2018.